Young-Type Interference in Collisions between Hydrogen Molecular Ions and Helium

L. Ph. H. Schmidt,[1] S. Schössler,[1] F. Afaneh,[2] M. Schöffler,[1] K. E. Stiebing,[1] H. Schmidt-Böcking,[1] and R. Dörner[1]

[1]*Institut für Kernphysik, Goethe-Universität, Max-von-Laue-Straße 1, D-60438 Frankfurt am Main, Germany*

[2]*Physics Department, The Hashemite University, P.O. Box 150459, Zarqa 13115, Jordan*

(Received 27 June 2008; published 24 October 2008)

The dissociative electron transfer from He into 10 keV H_2^+ was measured in a kinematically complete experiment by using the cold target recoil ion momentum spectroscopy imaging technique in combination with a highly resolving molecular fragment imaging technique. The electron transfer into the dissociative $b^3\Sigma_u^+$ state of H_2 could be selected by kinematic conditions. We find a striking double slit interference pattern in the transverse momentum transfer which we can modify by selecting different internuclear distances. Compared to an optical double slit, interference minima and maxima are interchanged. The latter is the result of a phase shift in the electronic part of the wave function.

DOI: 10.1103/PhysRevLett.101.173202 PACS numbers: 34.50.−s, 34.70.+e, 34.80.Ht

The wave property of light was demonstrated more than 200 years ago by Thomas Young by measuring the interference behind a double slit. In 1956, Möllenstedt and Düker [1] succeeded in performing a double slit experiment using electrons with an energy of about 100 eV. Similar experiments with atoms and molecules are challenging because at room temperature atoms have a wavelength on the order of the Bohr radius. Carnal and Mlynek [2] were the first to demonstrate double slit interference for slow metastable He, which had a de Broglie wavelength of about 0.1 nm, by using two slits separated by 8 μm.

Ion beams as they are provided by common ion sources have several keV kinetic energy, and therefore the de Broglie wavelength is several orders of magnitude smaller. Therefore, demonstrating Young-type interference for such high energetic beams requires a double slit as narrow as the internuclear distance of molecules.

The idea of interference in collisions of ions with molecules was first discussed by Tuan and Gerjuoy [3]. They suggested that the incoming projectile wave scatters from both atomic centers producing an interference pattern for the outgoing waves. They found that the cross section of electron transfer from hydrogen molecules into fast protons can be described by a scattering amplitude which is the coherent sum of two transition amplitudes corresponding to the atomic centers (see [4–8] for later work following this idea).

The double slit analogy suggests that the axis of the molecule which forms the double slit has to be fixed in space to obtain interference in the scattering pattern of the projectile. The above theoretical work and subsequent experimental work, however, showed that other global observables show traces of this interference [9–13].

In this Letter, we demonstrate the originally proposed direct double slit situation by measuring the scattering angles for fixed molecular orientations. It turns out to be much richer than anticipated in the literature so far since electronic degrees of freedom strongly affect the interference. Technically, it is extremely difficult to resolve the interference structure by a projectile scattering angle measurement. We have therefore performed a corresponding experiment in inverse kinematics. The dissociative electron transfer into singly charged hydrogen molecules was measured:

$$H_2(1s\sigma)^+ + He(1s^2) \rightarrow H_2^* + He^+ \rightarrow H + H + He^+. \quad (1)$$

Besides the fact that the molecule is now the projectile instead of the target, the direction of the electron transfer is inversed. Nevertheless, it can be expected that the interference should still be present as predicted by Tuan and Gerjuoy [3].

The experiment was carried out by crossing a collimated beam of 10 keV H_2^+ ions with a supersonic He gas jet at an angle of 90°. 810 mm behind this reaction region, the neutral fragments of the projectile were detected by a microchannel plate detector, while charged fragments were deflected out of the beam. In contrast to previous experiments [14], we used a hexagonal delay line anode to reduce the problem of multihit dead time at this detector [15]. The momentum vector of the ionized target atom was measured in coincidence with the molecular fragments by cold target recoil ion momentum spectroscopy [16,17] with a resolution better than 0.3 a.u. FWHM. Random coincidence background could be suppressed by checking for momentum conservation in the two dimensions perpendicular to the beam axis.

The reaction (1) includes several pathways. Since electronic and nuclear degrees of freedom are coupled, a summation over electronic states would obscure the sought-after interference in the nuclear scattering. Therefore, we start the discussion with the determination of the dissociation pathway and electronic degrees of freedom before focusing on the interferences.

Our projectile velocity of $v_p = 0.447$ a.u. leads to a collision time of a few hundred attoseconds, while the

dissociation of the molecule is much slower (a.u. denotes atomic units: $m_e = \hbar = e = c/137 = 1$). Therefore, the electron transfer and the dissociation can be treated as two successive independent steps. In the first step, several electronic states of the neutral molecule can be populated which requires the energy $-Q$ taken from the relative motion between the helium and the molecule. It is determined from the recoil ion momentum in the direction of the beam axis $p_{z,\mathrm{He}}$.

The second step of the reaction is the dissociation, which converts part of the electronic excitation energy of the H_2 molecule into kinetic energy release (KER). Figure 1 shows the measured KER distribution versus the $-Q$ value. Most events are found on diagonal lines (KER + Q = const). Deviations from the diagonal lines result from the experimental Q resolution of 1.5 eV, the initial vibrational excitation of the H_2^+ molecules gained in the ion source with energies up to 2.5 eV, and from radiative transitions [structures along the vertical lines (I) and (II) with KER below 7 eV; see [14]].

Line (a) corresponds to the case where all particles are in their electronic ground state. Electronic excitation results in lines (b)–(f). In the following we focus on events along line (a), i.e., dissociation into H(1s) + H(1s). Two potential energy curves converge to this dissociation limit: $X^1\Sigma_g^+$ is binding and dissociates only if the nuclear motion is excited into the vibration continuum which results in very small KER below 1 eV. $b^3\Sigma_u^+$ $2p\sigma$ is repulsive and leads to KER from nearly zero up to 8 eV. This KER corresponds to internuclear distances R between 0.06 and 0.26 nm. This wide range of R is accessible for Franck-Condon transitions because of the vibrational excitation of the H_2^+.

Ground state hydrogen atoms can also be produced by predissociation where bound excited states decay by converting the electronic excitation energy completely into

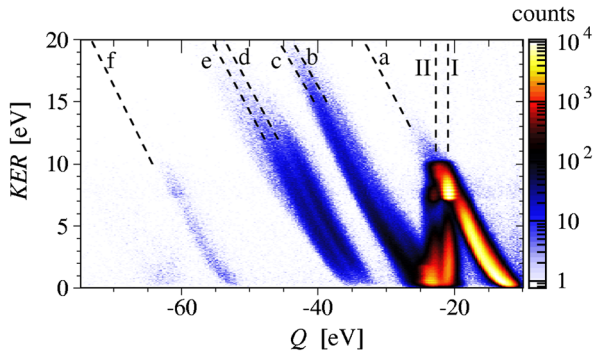

FIG. 1 (color online). Energy correlation diagram: The number of counts as a function of $Q = -v_p p_{z,\mathrm{He}} - 0.5 m_e v_p^2$ and KER is shown on a logarithmic color scale. The diagonal lines with a constant sum of KER and Q correspond to a specific electronic final state $\mathrm{H}(n_1 l) + \mathrm{H}(n_2 l) + \mathrm{He}(ml)^+$: (a) $n_1 = n_2 = m = 1$; (b) $n_1 = 2$, $n_2 = m = 1$; (c) $n_1 \geq 3$, $n_2 = m = 1$; (d) $n_1 = n_2 = 2$, $m = 1$; (e) $n_1 \geq 3$, $n_2 = 2$, $m = 1$; (f) $n_1 = n_2 = 1$, $m = 2$.

KER. Those events are dominantly found at KER above 7 eV [see line (a) in Fig. 1; compare [14]]. By selecting events along line (a) (-15 eV $< Q +$ KER < -10 eV) with KER between 1 and 5 eV, we pick only the direct electron transfer from He($1s^2$) into the $2p\sigma$ orbital of the hydrogen molecule.

Having completely determined the electronic degrees of freedom, we now turn to the two-center interference in the nuclear scattering, the key result presented in our Letter. For this discussion, it is most helpful to switch into the moving coordinate frame of the H_2^+ projectile. In this frame, the molecule acts as the scattering center, and the He is the projectile which scatters at the molecule.

The de Broglie wavelength of the He is given by $\lambda_{\mathrm{He}} = h/(m_{\mathrm{He}} v_p) = 0.0019$ a.u. This wave scatters at the two identical centers separated by R, and we will show that the scattering pattern consists of interference structures of two spherical waves originating from the two scattering centers. Such scattering patterns are shown in Fig. 2. In Figs. 2(a) and 2(c), two different internuclear distances are selected via the KER and the molecule is oriented 90° to the beam axis, while in Fig. 2(b) an angle of 55° to the beam axis is selected. Instead of scattering angles α, we show transversal momenta $p_{r,\mathrm{He}}$. In the molecular frame of reference, a typical momentum transfer of 3 a.u. corresponds to $\alpha = p_{r,\mathrm{He}}/m_{\mathrm{He}} v_p = p_{r,\mathrm{He}}/3300\,\mathrm{a.u.} = 0.9\,\mathrm{mrad}$. The coordinates used are shown in Fig. 2(d), z' is the beam direction, and the $x'z'$ plane is defined by the beam and the molecular axis. In Figs. 2(a)–2(c), the projection of the molecular axis onto the displayed plane is horizontal. Impact parameters smaller than the internuclear distance lead to large transverse momentum transfer. Therefore, interference fringes resulting from the two-center character of the molecule are expected to appear at the outer area.

An optical double slit experiment with size and wavelength as in Figs. 2(a) and 2(c) would show interference maxima at the positions which are indicated by the thick vertical lines. In our observed structure, the positions of maxima and minima are clearly inverted compared to the optical case. This is, in particular, striking at $p_{x',\mathrm{He}} = 0$, where an optical double slit leads to a zero order maximum while our observed pattern has a nodal line. This inversion of fringes to antifringes clearly proves an additional phase shift of π between the two scattering centers.

As discussed above, we selected those events where the electron is captured into the $2p\sigma_u$ orbital of the molecule. This state has equal contributions but opposite phase at both nuclei. Populating this state by an electron extracted from the He generates outgoing He^+ waves, which also have opposite phases for scattering at the two molecular centers. For close collisions and molecules oriented perpendicular to the beam axis, the superposition of these two waves results in an interference pattern inverted to the optical analogue.

The contribution in the center of Figs. 2(a)–2(c) has small $p_{r',\mathrm{He}}$ and results from large impact parameters far

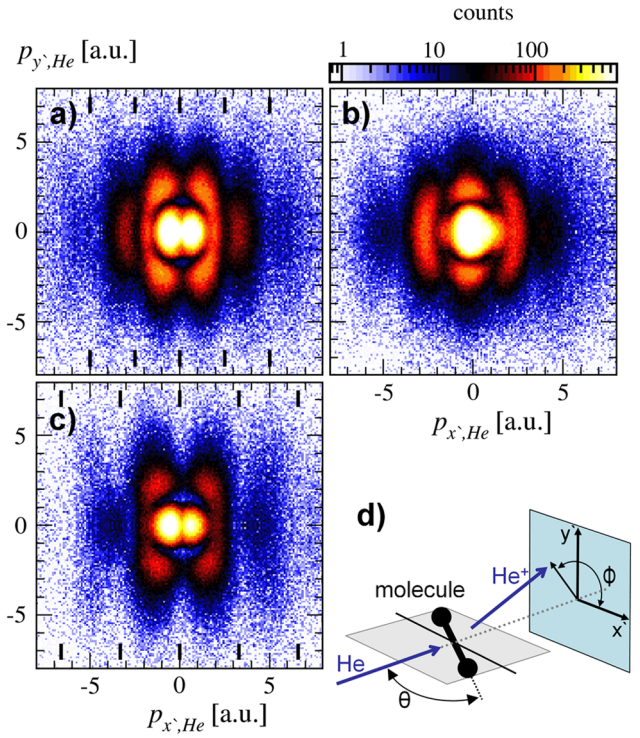

FIG. 2 (color online). Helium scattering pattern $d^2\sigma/(dp_{x',\mathrm{He}}, dp_{y',\mathrm{He}})$ of the reaction $\mathrm{He}(1s^2) + \mathrm{H}_2^+(1s\sigma) \rightarrow \mathrm{He}(1s)^+ + \mathrm{H}(1s) + \mathrm{H}(1s)$ in the plane perpendicular to the beam direction (z' axis). By the relative momenta of the molecular fragments, we selected events with different internuclear distances and different angles θ between the molecular axis and the beam direction from the data: (a) $80° < \theta < 90°$, 1 eV < KER < 2 eV. This corresponds to 2.9 a.u. > R > 2.3 a.u. (b) $50° < \theta < 60°$ and 1 eV < KER < 2 eV. (c) $80° < \theta < 90°$ and 3 eV < KER < 4 eV (corresponds to 2 a.u. > R > 1.7 a.u.). The thick vertical lines show the positions where interference maxima are expected for the coherent scattering at the two molecular centers. The experimental data have been mirrored at the horizontal axis in order to reduce the statistical error.

outside the molecule. Those events do not probe the two-center structure of the molecule. Nevertheless, in the case of molecular orientation perpendicular to the beam axis [Figs. 2(a) and 2(c)], this contribution shows a nodal line at $p_{x',\mathrm{He}} = 0$. Since at this specific orientation $x' = 0$ describes a symmetry plane of the molecule, this node is related to the symmetry change from g to u of the electronic wave function of the molecule.

Between the contribution in the center and the interference fringes, a circle of minimum intensity is found at about $p_{r',\mathrm{He}} = 1.6$ a.u. It does not vary with KER and molecular orientation. Similar structures also appear at p + He collisions. This minimum is not caused by the two-center structure of the molecule.

Next we will discuss the interference pattern for those cases where the molecule is not oriented perpendicular to the projectile beam, i.e., θ much smaller than 90°. All interference stripes seem to be shifted to the right which indicates additional contributions to the phase shift β between the two scattering pathways. For a quantitative comparison between our experimental data and a simple model, we extracted events with fixed θ, KER, and $p_{r',\mathrm{He}}$ to get one-dimensional distributions $d\sigma/d\phi$ shown in Fig. 3. These distributions represent fourfold differential cross sections which correspond to the intensity along a circle with radius $p_{r',\mathrm{He}}$ in Fig. 2.

The left column [Figs. 3(a), 3(d), and 3(g)] corresponds to the standard double slit geometry, where the connection axis between the scattering centers is oriented perpendicular to the incoming beam ($\theta = 90°$). It shows three different choices of R and $p_{r',\mathrm{He}}$. The fringe separation scales with internuclear distance as expected from an optical double slit. The middle and right columns show different tilt angles θ of the molecule to the beam axis. This allows us to measure possible phase shifts induced in the collision.

Our model calculates the differential cross section as a coherent superposition of scattering at the two centers resulting in

$$d\sigma/d\phi = \mathrm{const} \times \cos^2(\beta/2). \quad (2)$$

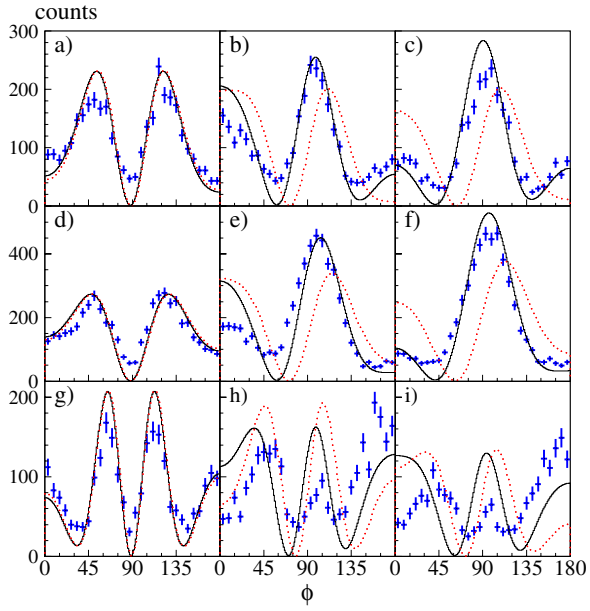

FIG. 3 (color online). Cross section for various collision parameters in dependence of the angle ϕ [as shown in Fig. 2(d)]. Measured data are shown as blue dots. The solid line is calculated using the full theory and the dotted red line by using a simpler model (for details see text). In each panel, the theoretical curves are normalized to the respective data. The left column represents collisions with an angle θ (between molecule and beam axis) of 85°–90°, the middle column of 55°–60°, and the right column of 45°–50°. The three rows show data for different $p_{r',\mathrm{He}}$ and KER as follows: (a)–(c) 2.2 a.u. < $p_{r',\mathrm{He}}$ < 2.4 a.u. and 1.5 eV < KER < 2 eV; (d)–(f) 2.2 a.u. < $p_{r',\mathrm{He}}$ < 2.4 a.u. and 2 eV < KER < 3 eV; (g)–(i) 3.5 a.u. < $p_{r',\mathrm{He}}$ < 3.7 a.u. and 2 eV < KER < 3 eV.

Hereby the phase shift β between the two contributions is calculated as

$$\beta = \pi + \mathbf{R} \cdot \Delta\mathbf{p}_{\mathrm{He}}\hbar^{-1} + \Delta E \Delta t \hbar^{-1}. \quad (3)$$

The term π stems from the inversion of the molecular symmetry from even to odd as discussed above.

The change in He momentum $\Delta\mathbf{p}_{\mathrm{He}}$ leads to a change of the de Broglie wavelength and is considered by the second term of Eq. (3), which is consistent with the theoretical description of Tuan and Gerjuoy [3]. Representing the scalar product of the second term by its components results in

$$\mathbf{R} \cdot \Delta\mathbf{p}_{\mathrm{He}} = p_{z',\mathrm{He}} R\cos(\theta) + p_{r',\mathrm{He}}\cos(\phi) R\sin(\theta). \quad (4)$$

We used $R_{y'} = 0$ and $p_{x',\mathrm{He}} = p_{r',\mathrm{He}}\cos(\phi)$ resulting from the definition of the coordinate system. At high projectile velocity, $p_{z',\mathrm{He}}$ is dominated by the transferred electron momentum $m_e v_p$. In our case of low v_p and close collisions, however, the transversal component $p_{r',\mathrm{He}}$ is much higher than $m_e v_p$. In Fig. 3, the term $p_{z',\mathrm{He}} R\cos(\theta)$ shows up as a constant phase contribution, i.e., a shift of the peaks, which depends on KER by its correlation to Q and R.

The third term $\Delta E \Delta t \hbar^{-1}$ of Eq. (3) has not been discussed in the literature so far. In a time-dependent description of a moving quantum mechanical particle, the kinetic energy contributes to the total energy E of the system. The time-dependent wave function $\Psi'(\mathbf{r}, t)$ can be calculated from the stationary solution $\Psi(\mathbf{r})$ by multiplying it with a so-called translation factor [4]:

$$\Psi'(\mathbf{r}, t) = \Psi(\mathbf{r} - \mathbf{v}t) e^{(i\mathbf{p}\cdot\mathbf{r}\hbar^{-1} - iE t\hbar^{-1})}. \quad (5)$$

The helium wave reaches the two scattering centers which are separated by R with a time difference $\Delta t = R\cos(\theta)/v_p$. Caused by the reaction with the molecule, the energy of the helium is changed by ΔE, which is deduced from the energy transferred to the molecule $\mathrm{KER} + \varepsilon_{H_2^+} - 2\varepsilon_{\mathrm{H}} = \mathrm{KER} + 10.9$ eV ($\varepsilon_{H_2^+}$ and ε_{H} are the binding energies of the quoted particles). Initial vibration energy is neglected but would give only a minor contribution to this energy. The helium momentum is changed by $\Delta\mathbf{p}_{\mathrm{He}}$. Comparing the initial and final state translation factors of both pathways results in the second and third phase terms of Eq. (3).

The angle ϕ effects the phase only by the second term of Eq. (3). Therefore the spectra in Fig. 3 allow dissecting this phase contribution from the two other terms by analyzing the peak positions. We compare the experimental data (dots) with two theoretical curves. The solid lines in Fig. 3 are calculated as described by Eqs. (2)–(4). Neglecting the phase contribution $\Delta E \Delta t \hbar^{-1}$ results in the dotted red line. In the spectra shown in the left column, the two theoretical curves coincide because Δt is small for this molecular orientation ($\theta = 90°$). For the middle column we selected $\theta = 57.5° \pm 2.5°$ and for the right $\theta = 47.5° \pm 2.5°$. The three rows differ by the selected KER and $p_{r',\mathrm{He}}$. The central peak is much better described by the full theory which indicates that the phase contribution resulting from the time dependence of the system cannot be neglected.

In both models, R is simply calculated from KER using the potential energy curve $b^3\Sigma_u^+$. This approximation neglects initial vibrational excitation and the enhancement of KER by high momentum transfer $p_{r',\mathrm{He}}$. Therefore the R used by our model is only a crude approximation, which results in discrepancies mainly seen at $\phi = 0°$ and 180° in Figs. 3(h) and 3(i) where higher $p_{r',\mathrm{He}}$ are selected.

In conclusion, we have experimentally demonstrated a Young-type interference in collisions of atoms with fixed-in-space molecules. We demonstrated the variation of the fringe separation with the internuclear distance. The scattering process of composite massive systems is shown to be much richer than its optical analogue. While the interference is found in the motion of the He, the change of the internal electronic degrees leads to a strong modification of the interference pattern. The symmetry changes of the electronic wave functions invert interference fringes to antifringes. The excitation energies lead to phase shifts which are experimentally accessible by tilting the slit. The richness of the observed phenomena invites more theoretical work aiming for a unified full quantum treatment.

This work was supported by Deutsche Forschungsgemeinschaft and RoentDek GmbH.

[1] G. Möllenstedt and H. Düker, Z. Phys. **145**, 377 (1956).
[2] O. Carnal and J. Mlynek, Phys. Rev. Lett. **66**, 2689 (1991).
[3] T. F. Tuan and E. Gerjuoy, Phys. Rev. **117**, 756 (1960).
[4] R. Shingal and C. D. Lin, Phys. Rev. A **40**, 1302 (1989).
[5] N. C. Deb *et al.*, Phys. Rev. A **38**, 3769 (1988).
[6] Y. D. Wang *et al.*, Phys. Rev. A **40**, 3673 (1989).
[7] S. E. Corchs *et al.*, Phys. Rev. A **47**, 201 (1993).
[8] M. E. Galassi, R. D. Rivarola, and P. D. Fainstein, Phys. Rev. A **70**, 032721 (2004).
[9] S. Martinez *et al.*, Phys. Rev. A **72**, 062722 (2005).
[10] K. Støchkel *et al.*, Phys. Rev. A **72**, 050703(R) (2005).
[11] I. Reiser, C. L. Cocke, and H. Bräuning, Phys. Rev. A **67**, 062718 (2003).
[12] S. Cheng *et al.*, Phys. Rev. A **47**, 3923 (1993).
[13] N. Stolterfoht *et al.*, Phys. Rev. A **69**, 012701 (2004).
[14] D. P. Bruijn *et al.*, Chem. Phys. **85**, 215 (1984).
[15] O. Jagutzki *et al.*, IEEE Trans. Nucl. Sci. **49**, 2477 (2002).
[16] J. Ullrich *et al.*, Rep. Prog. Phys. **66**, 1463 (2003).
[17] W. Wu, M. H. Prior, and H. Bräuning, Phys. Rev. A **57**, R5 (1998)